Theor Chem Acc (2000) 104:471–483
DOI 10.1007/s002140000175

Theoretical
Chemistry Accounts

Regular article

Particular and homogeneous solutions of time-independent wavepacket Schrödinger equations: calculations using a subset of eigenstates of undamped or damped Hamiltonians

Srinivasan S. Iyengar[1], **Donald J. Kouri**[1], **David K. Hoffman**[2]

[1] Department of Chemistry and Department of Physics, University of Houston, Houston, TX 77204-5641, USA
[2] Department of Chemistry and Ames Laboratory, Iowa State University, Ames, IA 50011, USA

Received: 29 February 2000 / Accepted: 5 April 2000 / Published online: 18 August 2000

Abstract. A variety of causal, particular and homogeneous solutions to the time-independent wavepacket Schrödinger equation have been considered as the basis for calculations using Chebychev expansions, finite-τ expansions obtained from a partial Fourier transform of the time-dependent Schrödinger equation, and the distributed approximating functional (DAF) representation for the spectral density operator (SDO). All the approximations are made computationally robust and reliable by damping the discrete Hamiltonian matrix along the edges of the finite grid to facilitate the use of compact grids. The approximations are found to be completely well behaved at all values of the (continuous) scattering energy. It is found that the DAF–SDO provides a suitable alternative to Chebychev propagation.

Key words: Time-independent wavepackets – Distributed approximating functionals – Spectral density operator – Eigen function calculations of scattering amplitudes

1 Introduction

The fundamental equation in nonrelativistic quantum mechanics is the time-dependent Schrödinger equation (TDSE)

$$\imath\hbar\frac{\partial}{\partial t}|\chi(t)\rangle = H|\chi(t)\rangle \ , \tag{1}$$

where $|\chi(t)\rangle$ is the ket vector describing the scattering system. The formal solution to this equation (for H independent of time), namely,

$$|\chi(t)\rangle = \exp\left(-\frac{\imath Ht}{\hbar}\right)|\chi(0)\rangle \ , \tag{2}$$

where $|\chi(0)\rangle$ describes the initial state of the system, is the starting point for many time-dependent approaches [1–4]. It is also well known that the complete ($-\infty$ to $+\infty$) time-to-energy Fourier transform of Eq. (1) for energies in the continuum gives rise to the homogeneous, time-independent Schrödinger equation (TISE) [5], which along with its integral (Lippmann–Schwinger, LS) [6] form has been the 'workhorse' equation of scattering calculations in physics and chemistry.

It has been shown that the time-to-energy transform of Eq. (2) produces a scattering eigenstate of the TISE obeying causal boundary conditions if the coordinate representation wavefunction, $\langle\vec{r}|\chi(0)\rangle$, is 'precollisional' [7–11]. By this is meant that $V(\vec{r})\langle\vec{r}|\chi(t)\rangle$ is (effectively) zero over all coordinate space for all times $t < 0$. Here, $V(\vec{r})$ is the scattering potential. That is, the wavepacket has not encountered the scattering potential in its prehistory. The Fourier components of $\langle\vec{r}|\chi(0)\rangle$ at energy E determine the appropriate boundary conditions. (Likewise, if $\langle\vec{r}|\chi(0)\rangle$ is 'postcollisional', the time-to-energy transform of Eq. (2) produces a solution to the TISE that obeys anticausal boundary conditions.)

It is only recently that 'half'-Fourier time-to-energy transforms have been exploited in quantum scattering [7–11] (which is somewhat surprising since they have long been used for the quantum Liouville/Von Neumann equation [12, 13] in statistical mechanics [14, 15]). The half-Fourier transform of Eq. (2), integrating from $t = 0$ to ∞, gives rise to the state vector

$$|\xi^+\rangle = \frac{1}{(E^+ - H)}|\chi(0)\rangle \ , \tag{3}$$

where $(E^+ - H)^{-1}$ is the causal Green function. Since the ket vector, $|\xi^+\rangle$, explicitly depends on the initial vector,

Present address: S. S. Iyengar, Center for Nanoscale Science and Technology, Rice Quantum Institute and Department of Chemistry, Mail Stop 60, Rice University, Houston, TX 77005-1892, USA
Correspondence to: D. J. Kouri, e-mail: kouri@uh.edu

$|\chi(0)\rangle$, which in the coordinate representation is the initial wavepacket, Eq. (3) is termed the time-independent wavepacket (TIW) equation [7–11]. Although $|\xi^+\rangle$ is not a scattering eigenstate, it turns out that it does have a very simple physical interpretation if $|\chi(0)\rangle$ is precollisional [7–11]. More important, all relevant scattering information can be extracted from $|\xi^+\rangle$ at energies contained in the initial wavepacket, $|\chi(0)\rangle$. In fact $|\xi^+\rangle$ has exactly the same scattering information content as the improper eigenket resulting from the full time-to-energy Fourier transform, as should be no surprise since the integral from $t = 0$ to ∞ includes all times that the packet overlaps the potential. Similarly,

$$|\xi^-\rangle = \frac{1}{(E^- - H)}|\chi(0)\rangle \ , \tag{4}$$

where $(E^- - H)^{-1}$ is the anticausal Green function and $|\chi(0)\rangle$ is postcollision, has the information content of the corresponding anticausal eigenstate, and is obtained from the half-Fourier transform of Eq. (2), integrating from $t = 0$ to $-\infty$. Both of these TIW kets are clearly particular solutions of the inhomogeneous time-independent wavepacket Schrödinger equation (TIWSE),

$$(E - H)|\xi\rangle = |\chi(0)\rangle \ . \tag{5}$$

The general solution to this inhomogeneous equation is [16, 17]

$$|\xi\rangle = G^{\mathrm{P}}(E)|\chi(0)\rangle + \lambda\delta(E - H)|\chi(0)\rangle \ , \tag{6}$$

where λ is an arbitrary constant, $G^{\mathrm{P}}(E)$ is the principal value of the Green function and $\delta(E - H)$ is the spectral density operator (SDO). The ket vector $G^{\mathrm{P}}(E)|\chi(0)\rangle$ is a particular solution and $\delta(E - H)|\chi(0)\rangle$ is the solution to the homogeneous equation (the TISE). From the well-known expression [16]

$$G^{\pm}(E) = G^{\mathrm{P}}(E) \mp \imath\pi\delta(E - H) \tag{7}$$

it is clear that Eqs. (3) and (4) are, indeed, special cases of Eq. (6). Related methods based on these equations have been used by several other groups recently for scattering calculations [18–20].

Equations (3) and (4) have an important advantage over the LS equation for extracting scattering information, namely, all of the explicit energy dependence is in the Green function $(E^{\pm} - H)^{-1}$. By contrast, in the LS equation the scattered wave is given by $(E^+ - H)^{-1}V|\phi\rangle$, where $|\phi\rangle$ is an eigenstate of $(H - V)$ at energy E. Thus, in the LS equation there is an additional explicit energy dependence in $|\phi\rangle$, whereas, in Eq. (3), the causal Green function acts on the same ket vector, $|\chi(0)\rangle$, at all energies.

In this article, we consider various approximate solutions to a novel TIWSE, which is derived from a partial-finite Fourier transform of the TDSE. Approximate solutions to the standard TIWSE are also considered, with the basic approximation being the replacement of the exact, continuous Hamiltonian with a finite-dimensional, discrete matrix. To obtain reliable results, it is crucial that the 'box' introduced to discretize and truncate the Hamiltonian be large enough that interference effects produced by scattering at the boundaries be controllably small in the region where the final state analysis is carried out. Furthermore, in all cases, the action of the relevant dynamical operator (which is a function of the finite, discrete Hamiltonian matrix) on an initial wavepacket is approximated in terms of only a subset of the eigenstates of the finite, discrete Hamiltonian matrix. All calculations are made more robust by the introduction of damping to facilitate the use of smaller, more compact boxes [19]. The accuracy and computational effectiveness of the approximations are studied for a one-dimensional scattering problem, by calculating scattering information for a wide range of energies, including energies that are exactly equal to eigenvalues of the discrete Hamiltonian matrix.

The article is organized as follows. In Sect. 2 we consider various generalizations of, and formal solutions to, the TIW quantum equations, based on partial-finite Fourier transforms of the TDSE. In Sect. 3 we present computational strategies based on the use of eigenstates of the discrete Hamiltonian, to obtain solutions to the equations derived in Sect. 2. In Sect. 4 we present results of calculations for a one-dimensional box containing an Eckart barrier, and in Sect. 5 we discuss our results.

2 Generalizations of the TIWSE

To derive a general TIWSE [7], we multiply the TDSE in Eq. (1) by $(\mathrm{d}t/2\pi\hbar)\exp(\imath Et/\hbar)$ and integrate between two finite times, t_1 and t_2 (where $[t_1, t_2]$ is the time interval for the scattering experiment), so that

$$\frac{1}{2\pi\hbar}\int_{t_1}^{t_2}\mathrm{d}t\exp\left(\frac{\imath Et}{\hbar}\right)\left(\imath\hbar\frac{\partial}{\partial t}|\chi(t)\rangle = H|\chi(t)\rangle\right) \ . \tag{8}$$

Then integrating the left-hand side by parts, we obtain

$$\begin{aligned}(E - H)\frac{1}{2\pi\hbar}\int_{t_1}^{t_2}\mathrm{d}t\exp\left(\frac{\imath Et}{\hbar}\right)|\chi(t)\rangle \\ = \frac{\imath}{2\pi}\exp\left(\frac{\imath Et_1}{\hbar}\right) \\ \times\left[1 - \exp\left(\frac{\imath(E - H)(t_2 - t_1)}{\hbar}\right)\right]|\chi(t_1)\rangle \ ,\end{aligned} \tag{9}$$

where from Eq. (2), we have used $|\chi(t_2)\rangle = \exp\left(-\frac{\imath H(t_2 - t_1)}{\hbar}\right)|\chi(t_1)\rangle$. We now define

$$|\xi(E)\rangle = \frac{1}{2\pi\hbar}\int_{t_1}^{t_2}\mathrm{d}t\exp\left(\frac{\imath Et}{\hbar}\right)|\chi(t)\rangle \ , \tag{10}$$

and introduce the relative time, $t' = t - t_1$, as the integration variable to obtain

$$\begin{aligned}|\xi(E)\rangle = \frac{1}{2\pi\hbar}\int_0^{\tau}\mathrm{d}t'\exp\left(\frac{\imath Et'}{\hbar}\right) \\ \times\left[\exp\left(\frac{\imath Et_1}{\hbar}\right)|\chi(t' + t_1)\rangle\right] \ ,\end{aligned} \tag{11}$$

where $\tau = t_2 - t_1$. In terms of these quantities, Eq. (9) becomes

$$(E-H)|\xi(E)\rangle = \frac{\imath}{2\pi}\left[1-\exp\left(\frac{\imath(E-H)\tau}{\hbar}\right)\right] \times \exp\left(\frac{\imath E t_1}{\hbar}\right)|\chi(t_1)\rangle \ . \quad (12)$$

Finally, we note that without loss of generality we can set $t_1 = 0$ (since the factor $\exp(\imath E t_1/\hbar)$ only contributes to the phase of the wavepacket at time t_1, which is in any case arbitrary). This leads to

$$(E-H)|\xi_\tau(E)\rangle = \frac{\imath}{2\pi}\left[1-\exp\left(\frac{\imath(E-H)\tau}{\hbar}\right)\right]|\chi(0)\rangle \ , \quad (13)$$

where the subscript τ in $|\xi_\tau(E)\rangle$ indicates the total propagation time.

A few comments regarding this new TIWSE, i.e., Eq. (13), are now in order. First, it is clear from Eq. (10) that $\langle\vec{r}|\xi_\tau(E)\rangle$ is the accumulation of the energy, E, component of the wavepacket at the point $\vec{r}$ over the propagation time, τ. Hence, at any point $\vec{r}$, the integral in Eq. (10) converges (i.e., becomes independent of τ) if at time τ the packet has forever passed over the point $\vec{r}$. Second, we note that in the limit $\tau \to \pm\infty$, the coordinate representation of the ket vector $[\exp(\imath(E-H)\tau/\hbar)|\chi(0)\rangle]$ must tend to zero at any finite $\vec{r}$, since the kinetic energy operator will eventually propagate the system away to infinity (provided the packet has zero overlap with any bound states of the Hamiltonian; this will always be true if the incident packet does not overlap the interaction region). Thus, from Eq. (13), we obtain

$$(E-H)|\xi(E)\rangle = \frac{\imath}{2\pi}|\chi(0)\rangle \quad (14)$$

in the limit as $\tau \to \pm\infty$, which is the standard TIWSE [7–11]. Hence, it is obvious that Eq. (14) is a special case of Eq. (13). Third, it is clear that Eq. (13) permits more general solutions than those provided by Eq. (10) (with $t_1 = 0$ and $t_2 = \tau$ as we have assumed) and these will be discussed later.

The formal solution to Eq. (13) is

$$|\xi_\tau(E)\rangle = \frac{\imath}{2\pi}\frac{1}{(E-H)} \times \left[1-\exp\left(\frac{\imath(E-H)\tau}{\hbar}\right)\right]|\chi(0)\rangle \ , \quad (15)$$

which is perfectly well behaved at all values of the energy, E, and for all packets, including those with bound state components. (That is, it does not give rise to singularities at any value of the energy, E, as is clear from a simple Taylor series expansion of the exponential term. Thus, there is no need to introduce $\pm\imath\epsilon$ to the energy in order to ensure the existence of $1/(E-H)$. This aspect will be illustrated in greater detail in the next section.) Furthermore, since [5, 16]

$$\lim_{\tau\to\pm\infty}\frac{1}{(E-H)}\left[1-\exp\left(\frac{\imath(E-H)\tau}{\hbar}\right)\right] = G^{\pm}(E) \ , \quad (16)$$

where $G^+(E)$ and $G^-(E)$ are the causal and anti-causal Green functions, respectively, the expression $\frac{1}{(E-H)}\left[1-\exp\left(\frac{\imath(E-H)\tau}{\hbar}\right)\right]$ can clearly be treated as an approximation to the causal (anti-causal) Green function for positive (negative) values of the finite propagation time, τ. Also, using Eq. (7), we note that the real part of Eq. (16) satisfies

$$\lim_{\tau\to\infty}\mathrm{Re}\left\{\frac{1}{(E-H)}\left[1-\exp\left(\frac{\imath(E-H)\tau}{\hbar}\right)\right]\right\} = \lim_{\tau\to\infty}\frac{1-\cos\frac{(E-H)\tau}{\hbar}}{E-H} = G^{\mathrm{P}}(E) \quad (17)$$

and the imaginary part of Eq. (16) satisfies

$$\lim_{\tau\to\infty}\mathrm{Im}\left\{\frac{1}{(E-H)}\left[1-\exp\left(\frac{\imath(E-H)\tau}{\hbar}\right)\right]\right\} = \lim_{\tau\to\infty}\frac{-\sin\frac{(E-H)\tau}{\hbar}}{E-H} = -\pi\delta(E-H) \ . \quad (18)$$

It is easy to verify [10] that $\frac{i}{2\pi}\delta(E-H)\chi(0)$ is a solution of the homogeneous TISE corresponding to evolution of the packet $\chi(0)$ from $t=-\infty$ to ∞.

3 Approximate solutions to the TIWSE

3.1 Finite-τ, distributed approximating functional and Chebychev approximations

In order to carry out calculations, we must evaluate the actions of $G^+(E)$, $G^{\mathrm{P}}(E)$ and $\delta(E-H)$ on an initial wavepacket, $|\chi(0)\rangle$. From the previous discussion it is clear that the action of these operators can be studied as a function of the finite propagation time, τ; i.e., specifically

$$G^+(E) \approx G^+_\tau(E) \equiv \frac{1}{E-H}\left(1-\exp\frac{\imath(E-H)\tau}{\hbar}\right) \ , \quad (19)$$

$$G^{\mathrm{P}}(E) \approx G^{\mathrm{P}}_\tau(E) \equiv \frac{1}{E-H}\left(1-\cos\frac{(E-H)\tau}{\hbar}\right) \quad (20)$$

and

$$\delta(E-H) \approx \delta_\tau(E-H) \equiv \frac{1}{\pi(E-H)}\sin\frac{(E-H)\tau}{\hbar} \quad (21)$$

may be used to evolve an initial wavepacket and study the behavior of the corresponding final states as a function of τ. Additionally, we may also consider approximating $\delta(E-H)$ in terms of the distributed approximating functionals (DAFs) [21–26]. For example, the Hermite–DAF approximation to the SDO, $\delta_M(E-H|\sigma)$, is given by

$$\delta(E-H) \approx \delta_M(E-H|\sigma) = \frac{1}{\sqrt{2\pi}\sigma}\exp\left(-\frac{(E-H)^2}{2\sigma^2}\right) \times \sum_{n=0}^{M/2}\left(-\frac{1}{4}\right)^n\frac{1}{n!}\,H_{2n}\left(\frac{E-H}{\sqrt{2}\sigma}\right) \ , \quad (22)$$

where the Hermite polynomials, $H_n(x)$, satisfy the recursion relation $H_{n+1}(x) = 2xH_n(x) - 2nH_{n-1}(x)$ and

M and σ are parameters whose choice determines how accurately $\delta_M(E-H|\sigma)$ approximates a Dirac delta function. For fixed $\sigma, M \to \infty$ produces the exact Dirac delta function. Similar to the case where $\delta(E-H)$ is approximated by a Chebychev expansion, this limit is related to the limit that the propagation time tends to infinity [10, 20]. However, the Hermite–DAF approximation to the Dirac delta function can also be viewed in terms of the limit $\sigma \to 0$ for fixed M. Similarly, this is an alternative way to achieve the infinite-propagation-time limit. In Sect. 4, we study this 'evolution', under the action of $\delta_M(E-H|\sigma)$, of an initial wavepacket as a function of σ for fixed M. Using other DAFs [27–31], for example the Gaussian–sinc–DAF operator [30], alternate expressions for $\delta(E-H)$ can be obtained. Further, if the Hamiltonian matrix is known to have symmetry, this symmetry can be exploited by constructing a representation for $\delta(E-H)$ using the symmetry-adapted DAF [31]. Typical behavior of the energy-to-time Fourier transform of the quantity $\delta_M(E|\sigma)$ (i.e., the corresponding time-domain filter) is presented in Fig. 1. Clearly, this quantity is a good approximation to the window function. Further, it may also be noted from Fig. 1 that as the value of σ decreases, the width of the window function increases, so a longer 'propagation time' results for the function to which $\delta_M(E-H|\sigma)$ is applied. Hence, as discussed in greater detail in Sect. 4, when the expression in Eq. (22) is applied on an initial wavepacket, it has the effect of modifying the wavepacket in the causal fashion when M is fixed and σ is reduced, i.e., the value of σ effectively correlates inversely with the time elapsed in the scattering process, just as the highest-degree Chebychev polynomial in expanding $\delta(E-H)$ correlates with the propagation time [10, 20].

In all the previous expressions, i.e. Eqs. (19)–(22), the final state results from the action of a function of the Hamiltonian on an initial wavepacket. This action may be approximated in many ways. For example, one could construct Chebychev polynomial approximations to each of the operators in Eqs. (19)–(22) [20, 32]. In this work we choose to resolve the initial wavepacket in terms of eigenstates of the Hamiltonian, thereby simplifying the procedure. That is,

$$|\xi_\tau^+(E)\rangle \equiv \frac{\imath}{2\pi} G_\tau^+(E)|\chi(0)\rangle \approx \frac{\imath}{2\pi} \sum_{j=J_{\min}}^{J_{\max}} \frac{1}{E-E_j}\left(1-\exp\frac{\imath(E-E_j)\tau}{\hbar}\right) \times |\phi_j\rangle\langle\phi_j|\chi(0)\rangle \ , \tag{23}$$

$$|\xi_\tau^{\mathrm{p}}(E)\rangle \equiv \frac{\imath}{2\pi} G_\tau^{\mathrm{p}}(E)|\chi(0)\rangle \approx \frac{\imath}{2\pi} \sum_{j=J_{\min}}^{J_{\max}} \frac{1}{E-E_j}\left(1-\cos\frac{(E-E_j)\tau}{\hbar}\right) \times |\phi_j\rangle\langle\phi_j|\chi(0)\rangle \ , \tag{24}$$

$$|\psi_\tau(E)\rangle \equiv \frac{\imath}{2\pi} \delta_\tau(E-H)|\chi(0)\rangle \approx \frac{\imath}{2\pi} \sum_{j=J_{\min}}^{J_{\max}} \frac{1}{\pi(E-E_j)} \times \sin\frac{(E-E_j)\tau}{\hbar}|\phi_j\rangle\langle\phi_j|\chi(0)\rangle \tag{25}$$

and

$$\psi_{M,\sigma}(E) \equiv \frac{\imath}{2\pi} \delta_M(E-H|\sigma)|\chi(0)\rangle \approx \frac{\imath}{2\pi}\frac{1}{\sqrt{2\pi}\sigma} \sum_{j=J_{\min}}^{J_{\max}} \exp\left[-\frac{(E-E_j)^2}{2\sigma^2}\right] \times \sum_{n=0}^{M/2}\left(-\frac{1}{4}\right)^n \frac{1}{n!} H_{2n}\left(\frac{E-E_j}{\sqrt{2}\sigma}\right) \times |\phi_j\rangle\langle\phi_j|\chi(0)\rangle \ , \tag{26}$$

where $\{E_j, \phi_j\}$ is the set of eigenvalues and eigenvectors of H and the values $J_{\min}$ and $J_{\max}$ are to be chosen such that the scattering energy, E, satisfies the 'minimal condition' inequality $E_{J_{\min}} < E < E_{J_{\max}}$. [Clearly, if the range $(E_{J_{\min}}, E_{J_{\max}})$ is increased to include the entire spectrum of the finite, discrete approximation to the Hamiltonian, all expressions on the right-hand side of Eqs. (23)–(26) attain their limiting values, which are still not exact since the Hamiltonian has been discretized and is finite-dimensional. However, in the limit of infinitesimal discretization, i.e., the continuous limit, the sums over j in the expressions become integrals and the associated expressions are formally exact.] In the case of the Hermite–DAF expression, $J_{\min}$ and $J_{\max}$ will be chosen such that $E_{J_{\min}}$ and $E_{J_{\max}}$ are relatively close to E, owing to the Gaussian damping factor $\exp\left(-\frac{(E-E_j)^2}{2\sigma^2}\right)$. The expressions in Eqs. (23)–(25) may, however, require a larger spread of $(E_{J_{\min}}, E_{J_{\max}})$ owing to the oscillatory nature of the (damped) trigonometric functions involved.

Alternative approximate expressions for the causal, particular and homogeneous solutions may be obtained by using the well-known Chebychev expansions [8, 33, 34], namely,

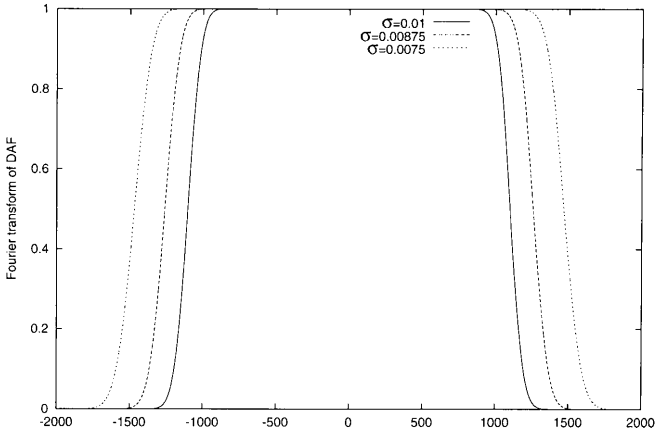

Fig. 1. Typical behavior of the Fourier transform of $\delta_M(E-E'|\sigma)$. As σ decreases, clearly the width of the square filter increases and, hence, a greater time range of the function on which $\delta_M(E-H|\sigma)$ is applied is retained

$$G^{\mathrm{P}}(E) \approx G_N^{\mathrm{P}}(E) = -\sum_{n=0}^{N} \frac{(2-\delta_{n0})\sin n\theta}{\Delta H \sin\theta}\, T_n(H_{\mathrm{norm}}) \qquad (27)$$

and

$$\delta(E-H) \approx \delta_N(E-H) = \sum_{n=0}^{N} \frac{(2-\delta_{n0})\cos n\theta}{\pi \Delta H \sin\theta}\, T_n(H_{\mathrm{norm}}) \ , \qquad (28)$$

where $\cos\theta = E_{\mathrm{norm}}$ and E_{norm}, H_{norm} and ΔH are the normalized [8, 35] energy, the normalized finite matrix representation of the Hamiltonian and its half-spectral width, respectively. Note again that the value of the highest-degree Chebychev polynomial is related to the length of time one propagates $\chi(0)$ in a time-dependent approach [10, 20]. The Chebychev polynomials are generated by the recursion relation [36]

$$T_n(H_{\mathrm{norm}}) = 2H_{\mathrm{norm}} T_{n-1}(H_{\mathrm{norm}}) - T_{n-2}(H_{\mathrm{norm}}) \ , \qquad (29)$$

where $T_0(H_{\mathrm{norm}}) = 1$ and $T_1(H_{\mathrm{norm}}) = H_{\mathrm{norm}}$. The actions of $G_N^{\mathrm{P}}(E)$ and $\delta_N(E-H)$ on an initial wavepacket may also be simplified by employing eigenstates of H_{norm}.

It must be noted that all these expressions may be employed directly only if the grid used for the scattering variable is large enough to prevent the wavepacket from reflecting off the ends of the grid. The results for smaller grids are bound to be affected because of boundary reflections of the wavepacket [19, 37]. Such reflections can be avoided by employing a Mandelshtam–Taylor damping scheme, which will now be discussed in more detail [19, 37].

3.2 'Damped' Hamiltonian approach to 'smoothed' TIW propagation

In general all calculations are performed within a box that contains the initial wavepacket and the potential. Application of the expressions of Sect. 3.1 results in propagation and eventual scattering of the initial wavepacket off the target potential. If the size of the box chosen is not 'large enough', the propagated waves will reflect off the walls of the box and reenter the scattering region to cause nonphysical interference behavior. If the box is 'large enough', scattering will be completed before the propagated waves reflect off the boundaries and reliable scattering information may be obtained. Further, since the box size affects the size of the matrices involved, smaller boxes result in smaller size matrices and hence shorter computation times. To facilitate the use of smaller boxes, we employ a Mandelshtam–Taylor scheme of damping the Hamiltonian matrix along the edges of the grid to reduce boundary reflections [19, 37]. The coordinate representation for the new 'damped Hamiltonian', $\tilde{H} = S^{1/2} H S^{1/2}$, is obtained using the diagonal (in the coordinate representation) damping matrix, $S^{1/2}$, whose elements are equal to 1 at all points on the grid except near the boundaries where they are gradually attenuated. Damping is enforced only where the potential is zero, and hence the potential energy is not damped. A typical form of $\langle x_i|S^{1/2}|x_i\rangle$ which is used in the calculations described later can be found in Fig. 2. (In a molecular beam experiment, damping can be thought of as cooling the system, so the beams, upon collision with the walls of the experimental setup, lose kinetic energy to the cold bath, condense on the walls of the chamber and do not get reflected back to the scattering region.) The operator $S^{1/2}$ resembles a filter in many ways, since it retains only the relevant portion of the Hamiltonian and, subsequently, the wavefunction.

The 'damped Hamiltonian' may be used directly in the expressions discussed in the previous section; however, for the Chebychev-based approximations, as was shown earlier [37], the Faber–Chebychev recursion [37–39] associated with such a 'damped Hamiltonian',

$$T_n(\tilde{H}_{\mathrm{norm}}) = 2\tilde{H}_{\mathrm{norm}} T_{n-1}(\tilde{H}_{\mathrm{norm}}) - (S^{1/2})^4 T_{n-2}(\tilde{H}_{\mathrm{norm}}) \ , \qquad (30)$$

with $T_0(\tilde{H}_{\mathrm{norm}}) = 1$ and $T_1(\tilde{H}_{\mathrm{norm}}) = \tilde{H}_{\mathrm{norm}}$, yields appropriate damped basis vectors for expanding various operators. This procedure [37] (of using the Faber–Chebychev recursion to evaluate operator functions of the damped Hamiltonian) is exactly equivalent to Mandelshtam and Taylor's implementation of the TIW formalism [7–11] by constructing $(E-H+\imath\epsilon)^{-1}$ using the known energy-dependent expansion coefficients [8, 33] but modifying the Chebychev recursion relation through the introduction of a damping factor. The procedure produces energy-independent basis vectors that decay exponentially in the boundary region [19]. It is also possible to use eigenstates of the damped Hamiltonian to evaluate expressions such as those outlined in Sect. 3.1.

We consider the coordinate representation of the action of a function of the damped Hamiltonian on one of its eigenstates, i.e., $f(\tilde{H})|\tilde{\phi}_j\rangle$. It can be arranged so that

$$\langle \vec{x}|f(\tilde{H})|\tilde{\phi}_j\rangle = \langle \vec{x}|f(\tilde{E}_j)|\tilde{\phi}_j\rangle \approx \langle \vec{x}|f(H)|\phi_j\rangle \qquad (31)$$

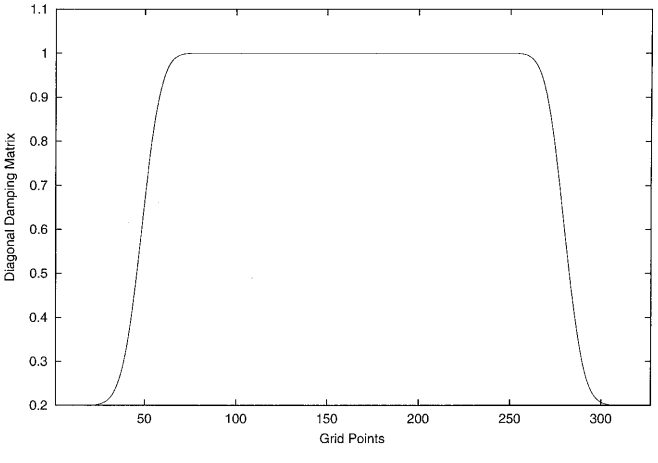

Fig. 2. Example of distributed approximating functional (*DAF*) damping matrix $S^{1/2}$. The Hamiltonian is damped smoothly along the edges of the grid for a box ranging from 1 to 327 grid points

holds to controllable accuracy for all values of the (discrete) position vector $\vec{x} \equiv \vec{x}_i$, where the damping-matrix element $\left[S^{1/2}\right]_{\vec{x}_i,\vec{x}_i} = 1$. This is chosen to be the case for the portion of the grid where the potential is nonzero, plus a large enough region for the final state analysis, so Eq. (31) is valid in the relevant scattering region. Thus, we are careful that the final state analysis for calculating various observables is also performed in a region which is separate from the damping region, so Eq. (31) is valid in this region of analysis as well. Hence the region of final state analysis and the physical scattering region are constrained not to overlap with the damping region, through the Hamiltonian matrix, and as long as this requirement is satisfied, Eq. (31) is valid.

The direct use of the damped Hamiltonian in the expressions involving the Chebychev polynomials, leads to Gibbs-phenomenon-like oscillations, which may be filtered out by 'smoothing' the polynomial expansions (by a process akin to low-pass filtering in digital signal processing [41]). To smooth the Chebychev approximations, we employ the diagonal Fourier space form of the DAF, which is known to be an arbitrarily accurate low-pass filter, so

$$\tilde{T}_n(E_{j,\mathrm{norm}}) = T_n(E_{j,\mathrm{norm}}) \exp\left(-\frac{(n\sigma')^2}{2}\right) \times \sum_{k=0}^{10}\left(\frac{1}{k!}\right)\left(\frac{(n\sigma')^2}{2}\right)^k , \tag{32}$$

where the value of σ' was chosen to be 0.0075, exactly as in Ref. [37].

The various dynamical states, in the region where the damping factor is 1, may then be expressed in terms of the action of functions of $\tilde{H}$ on the initial wavepacket. For example, we may obtain finite-τ approximations to the causal, particular and homogeneous solutions or DAF approximation to $\delta(E-H)$ by using the eigenstates of the damped Hamiltonian ($\tilde{H}$), $\{\tilde{E}_j, \tilde{\phi}_j\}$, and the 'smoothed' Hermite functions as

$$|\xi_\tau^+(E)\rangle \equiv \frac{\imath}{2\pi} G_\tau^+(E)|\chi(0)\rangle \approx \frac{\imath}{2\pi}\sum_{j=J_{\min}}^{J_{\max}} \frac{1}{E-\tilde{E}_j}\left(1-\exp\frac{\imath(E-\tilde{E}_j)\tau}{\hbar}\right) \times |\tilde{\phi}_j\rangle\langle\tilde{\phi}_j|\chi(0)\rangle \ , \tag{33}$$

$$|\xi_\tau^p(E)\rangle \equiv \frac{\imath}{2\pi} G_\tau^{\mathrm{P}}(E)|\chi(0)\rangle \approx \frac{\imath}{2\pi}\sum_{j=J_{\min}}^{J_{\max}} \frac{1}{E-\tilde{E}_j}\left(1-\cos\frac{(E-\tilde{E}_j)\tau}{\hbar}\right) \times |\tilde{\phi}_j\rangle\langle\tilde{\phi}_j|\chi(0)\rangle \ , \tag{34}$$

$$|\psi_\tau(E)\rangle \equiv \frac{\imath}{2\pi}\delta_\tau(E-\tilde{H})|\chi(0)\rangle \approx \frac{\imath}{2\pi}\sum_{j=J_{\min}}^{J_{\max}} \frac{1}{\pi(E-\tilde{E}_j)}\sin\frac{(E-\tilde{E}_j)\tau}{\hbar} \times |\tilde{\phi}_j\rangle\langle\tilde{\phi}_j|\chi(0)\rangle \tag{35}$$

and

$$|\psi_{M,\sigma}(E)\rangle \equiv \frac{\imath}{2\pi}\delta_M(E-\tilde{H}|\sigma)|\chi(0)\rangle \approx \frac{\imath}{2\pi}\frac{1}{\sqrt{2\pi}\sigma}\sum_{j=J_{\min}}^{J_{\max}} \exp\left(-\frac{(E-\tilde{E}_j)^2}{2\sigma^2}\right) \times \sum_{n=0}^{M/2}\left(-\frac{1}{4}\right)^n\frac{1}{n!}\tilde{H}_{2n}\left(\frac{E-\tilde{E}_j}{\sqrt{2}\sigma}\right) \times |\tilde{\phi}_j\rangle\langle\tilde{\phi}_j|\chi(0)\rangle, \tag{36}$$

where, as in Sect. 3.1, we have resolved the action of the relevant dynamical operators in terms of eigenstates restricted to the range $(E_{J_{\min}}, E_{J_{\max}})$. For the case of the Chebychev approximations, the final states can be expressed in terms of the action of $\tilde{T}_n(\tilde{H}_{\mathrm{norm}})$ on $|\chi(0)\rangle$ (i.e., in terms of the 'generalized scattering Krylov-like basis' $\{\tilde{\eta}_n\}$). As in Eqs. (30) and (31) we write the value of $|\tilde{\eta}_n\rangle$ on any grid point $\vec{x}_i$, where $\left[S^{1/2}\right]_{\vec{x}_i,\vec{x}_i} = 1$, as

$$\begin{aligned}|\tilde{\eta}_n\rangle &\equiv \tilde{T}_n(\tilde{H}_{\mathrm{norm}})|\chi(0)\rangle \\ &= 2\tilde{H}_{\mathrm{norm}}\tilde{T}_{n-1}(\tilde{H}_{\mathrm{norm}})|\chi(0)\rangle \\ &\quad - (S^{1/2})^4\tilde{T}_{n-2}(\tilde{H}_{\mathrm{norm}})|\chi(0)\rangle \\ &\approx \sum_{j=J_{\min}}^{J_{\max}} 2\tilde{E}_{j,\mathrm{norm}}\tilde{T}_{n-1}(\tilde{E}_{j,\mathrm{norm}})|\tilde{\phi}_j\rangle\langle\tilde{\phi}_j|\chi(0)\rangle \\ &\quad - (S^{1/2})^4\sum_{j=J_{\min}}^{J_{\max}}\tilde{T}_{n-2}(\tilde{E}_{j,\mathrm{norm}})|\tilde{\phi}_j\rangle\langle\tilde{\phi}_j|\chi(0)\rangle \ ,\end{aligned} \tag{37}$$

with $|\tilde{\eta}_0\rangle = |\chi(0)\rangle$ and $|\tilde{\eta}_1\rangle = \tilde{H}_{\mathrm{norm}}|\chi(0)\rangle$. The particular and homogeneous solutions to the TIWSE in the region devoid of damping are then given by

$$|\xi^{\mathrm{p}}(E)\rangle \equiv \frac{\imath}{2\pi}G_N^{\mathrm{P}}(E)|\chi(0)\rangle = -\frac{\imath}{2\pi\Delta H}\sum_{n=0}^{N}\frac{(2-\delta_{n0})\sin n\theta}{\sin\theta}\ |\tilde{\eta}_n\rangle \tag{38}$$

and

$$|\psi(E)\rangle \equiv \frac{\imath}{2\pi}\delta_N(E-H)|\chi(0)\rangle = \frac{\imath}{2\pi\Delta H}\sum_{n=0}^{N}\frac{(2-\delta_{n0})\cos n\theta}{\pi\sin\theta}\ |\tilde{\eta}_n\rangle \ , \tag{39}$$

where we have made use of the fact that the 'Chebychev polynomials' are given by [36] $T_n(x) = \cos\left(n\cos^{-1}x\right)$, and the angle θ is defined as in the previous section, i.e., $\cos\theta = E_{\mathrm{norm}}$. Note that strictly speaking, $\tilde{\eta}_n(\vec{x}) = \langle\vec{x}|\tilde{\eta}_n\rangle$ are not polynomials owing to the damping. Again, however, the damping region can be controlled so that Eq. (31) holds to the desired accuracy, justifying the use of Eqs. (38) and (39) prior to the damping region.

Clearly, there is a great variety of ways to generate scattering-type states, from which scattering information can be extracted.

3.3 Approximate scattering solutions at eigenvalues of H

It is interesting to note what happens to the expressions outlined previously when the continuous variable, E, is

exactly equal to one of the eigenvalues, $\tilde{E}_k$, of the discrete Hamiltonian matrix. When $E = \tilde{E}_k$, Eqs. (38) and (39), clearly, do not change. The expressions in Eqs. (24) and (25) (or, alternatively, Eqs. 34, 35), however, are functions of $1/(E - \tilde{E}_k)$, which is singular at $E = \tilde{E}_k$. This singularity, however, can be eliminated explicitly and we obtain

$$\begin{aligned}|\xi^{\mathrm{p}}_{\tau}(\tilde{E}_k)\rangle &\equiv \frac{\imath}{2\pi} G^{\mathrm{p}}_{\tau}(\tilde{E}_k)|\chi(0)\rangle \\ &= \frac{\imath}{2\pi}\sum_{j\neq k}\frac{1}{\tilde{E}_k - \tilde{E}_j}\left(1 - \cos\frac{(\tilde{E}_k - \tilde{E}_j)\tau}{\hbar}\right) \\ &\quad \times |\tilde{\phi}_j\rangle\langle\tilde{\phi}_j|\chi(0)\rangle \end{aligned} \tag{40}$$

and

$$\begin{aligned}|\psi_{\tau}(\tilde{E}_k)\rangle &\equiv \frac{\imath}{2\pi}\delta_{\tau}(\tilde{E}_k - H)|\chi(0)\rangle \\ &= \frac{\imath}{2\pi}\sum_{j\neq k}\frac{1}{\pi(\tilde{E}_k - \tilde{E}_j)}\sin\frac{(\tilde{E}_k - \tilde{E}_j)\tau}{\hbar} \\ &\quad \times |\tilde{\phi}_j\rangle\langle\tilde{\phi}_j|\chi(0)\rangle + \frac{\imath}{2\pi}\frac{\tau}{\hbar\pi}|\tilde{\phi}_k\rangle\langle\tilde{\phi}_k|\chi(0)\rangle \ . \end{aligned} \tag{41}$$

Using Eqs. (40) and (41) in Eq. (7), we obtain

$$\begin{aligned}|\xi^{+}_{\tau}(\tilde{E}_k)\rangle &\equiv \frac{\imath}{2\pi} G^{+}_{\tau}(\tilde{E}_k)|\chi(0)\rangle \\ &= \frac{\imath}{2\pi}\sum_{j\neq k}\frac{1}{\tilde{E}_k - \tilde{E}_j}\left[1 - \exp\frac{\imath(\tilde{E}_k - \tilde{E}_j)\tau}{\hbar}\right] \\ &\quad \times |\tilde{\phi}_j\rangle\langle\tilde{\phi}_j|\chi(0)\rangle + \frac{1}{2\pi}\frac{\tau}{\hbar}|\tilde{\phi}_k\rangle\langle\tilde{\phi}_k|\chi(0)\rangle \ . \end{aligned} \tag{42}$$

Similarly, using $E = \tilde{E}_k$ in Eq. (36), along with the analytical expression $H_{2n}(0) = (-1)^n 2^n (2n-1)!!$ [36], we obtain an expression for the DAF approximation to $\left[\delta(\tilde{E}_k - H|\sigma)\chi(0)\rangle\right]$ as

$$\begin{aligned}\psi_{M,\sigma}(\tilde{E}_k) &\equiv \frac{\imath}{2\pi}\delta_M(\tilde{E}_k - H|\sigma)|\chi(0)\rangle \\ &= \frac{\imath}{2\pi}\frac{1}{\sqrt{2\pi}\sigma}\sum_{j\neq k}\exp\left(-\frac{(\tilde{E}_k - \tilde{E}_j)^2}{2\sigma^2}\right) \\ &\quad \times \sum_{n=0}^{M/2}\left(-\frac{1}{4}\right)^n\frac{1}{n!}\,H_{2n}\left(\frac{\tilde{E}_k - \tilde{E}_j}{\sqrt{2}\sigma}\right) \\ &\quad \times |\tilde{\phi}_j\rangle\langle\tilde{\phi}_j|\chi(0)\rangle + \frac{\imath}{2\pi}\frac{1}{\sqrt{2\pi}\sigma} \\ &\quad \times \left(\sum_{n=0}^{M/2}\left(\frac{1}{2}\right)^n\frac{(2n-1)!!}{n!}\right) \\ &\quad \times |\tilde{\phi}_k\rangle\langle\tilde{\phi}_k|\chi(0)\rangle \ . \end{aligned} \tag{43}$$

We note that all these expressions are perfectly well behaved and finite. In the case of Chebychev expansions this reflects the fact that the usual $\epsilon \to 0_{\pm}$ limit, to select causal (anticausal) behavior, has been analytically carried out in obtaining the Chebychev expansion coefficients. In the case of Eqs. (40)–(42), the use of a finite-τ expression ensures that no singular behavior was ever introduced.

Finally, in the DAF expression, Eq. (43), the truncation of the Hermite sum, and the use of a finite width, σ, ensures a well-behaved approximation to the Dirac delta function.

The ability of the expressions studied here to yield correct results at any energy well within the eigenvalue range of the Hamiltonian contrasts with the '**R**'-matrix theory of nuclear reactions [16, 5, 40]. In that approach, one also diagonalizes the Hamiltonian inside a box but the expression used for the Green function is singular at the eigenenergies of the Hamiltonian.

4 Some illustrative computational tests and results

Our aim is twofold. First we evaluate the accuracy of the expressions derived in Sect. 3.1. We then assess the computational gains afforded by the use of damping and smoothing. For computational convenience, we consider a one-dimensional scattering problem of a wavepacket scattering off an Eckart barrier. The initial wavepacket is propagated inside a box using the various expressions derived here, which leads to the interaction and subsequent scattering of the wavepacket off the Eckart barrier potential. The 'final states' thus obtained are analyzed (using an analysis scheme outlined later in this section) to arrive at the transmission and reflection coefficients. Since the transmission and reflection coefficients across an Eckart barrier can be determined analytically [42] for any arbitrary energy of an incident plane wave, they are convenient for validating our results. The importance of damping and smoothing is studied by considering the effect on accuracy of varying the 'damped-box' size.

The discrete approximate representation for the kinetic energy part of the one-dimensional-box Hamiltonian is obtained on a uniform finite Cartesian grid using the DAFs [21–26]. (This is efficient because the DAF representation provides a highly banded, Toeplitz structure for the kinetic energy matrix.) The full Hamiltonian matrix then takes the form

$$\begin{aligned}H(x_{j'}, x_j) &= -\frac{\hbar^2\Delta x}{4\sqrt{2\pi}m\sigma_0^3}\exp\left(-\frac{(x_{j'} - x_j)^2}{2\sigma_0^2}\right) \\ &\quad \times \sum_{n=0}^{M/2}\left(-\frac{1}{4}\right)^n\frac{1}{n!}\,H_{2n+2}\left(\frac{x_{j'} - x_j}{\sqrt{2}\sigma_0}\right) \\ &\quad + \delta_{j'j}\frac{V_0}{\cosh^2\left(\frac{x_j - x_v}{a}\right)} \ , \end{aligned} \tag{44}$$

where the first term is the kinetic energy written using the 'second differentiating Hermite–DAF' and the second term is the (local) Eckart potential [42]. The $\{x_j\}$ are grid points in the one-dimensional box with uniform grid spacing, Δx, σ_0 is a width parameter associated with the Gaussian weight for the DAF kinetic energy, H_{2n+2} is a Hermite polynomial of degree $(2n+2)$ and $(M+2)$ is the highest degree of the Hermite polynomial used. The values for the parameters in the DAF (i.e., M and $\sigma/\Delta x$, as shown in Table 1) were chosen as in earlier studies to ensure that both the wavefunction and its second derivative were accurately

Table 1. Parameters used for the Hamiltonian matrix

Distributed approximating functional parameters		Eckart potential parameters		
$\frac{\sigma}{\Delta x}$	M	V_0	x_v	a
2.50	60	0.028215 au	0.0 Å	2.5 Å

calculated [7, 8]. For the Eckart potential, x_v is the center of the potential, a is its width parameter and V_0 is the maximum height of the Eckart barrier. All parameter values are given in Table 1.

4.1 The final state analysis

To obtain the transmission and reflection coefficients from the final propagated states, we sketch here a final state analysis specific to the present application. A more general and detailed treatment may be found elsewhere [37].

It is known that, by using a large enough region so that reflection at the walls does not occur [7–11] or by appropriately using absorbing boundary conditions [43–45], the solution (on the target side of the initial wavepacket) generated by the TIW approach is rigorously proportional to the LS causal solution. In the case of a finite box size, the final states obtained from the TIW analysis in the interior region where $\langle x|\chi(0)\rangle$ vanishes can be expressed as

$$|\xi\rangle = G(E)|\chi(0)\rangle = A|\psi^+_{+k}\rangle + B|\psi^+_{-k}\rangle \ , \tag{45}$$

where $|\psi^+_{+k}\rangle$ and $|\psi^+_{-k}\rangle$ are causal LS wave states with positive and negative momenta. Given appropriate values of A and B, the ket vector $|\xi\rangle$ may represent any of the expressions presented in Sect. 3. Since, in the one-dimensional case, it is arbitrary which side of the potential the initial wavepacket is on, further analysis in this section will assume it to be on the left. Further, due to the symmetry of the Eckart potential, the coefficient of reflection for the wave with positive momentum is the same as that for the wave with negative momentum. Hence, for a point x_r, located to the right (r) of the target,

$$\langle x_r|\psi^+_{+k}\rangle = T\exp(\imath k x_r) \ , \tag{46}$$

$$\langle x_r|\psi^+_{-k}\rangle = \exp(-\imath k x_r) + R\exp(\imath k x_r) \ , \tag{47}$$

where T and R represent the transmission and reflection coefficients. Similarly, for a point x_l in the region between the initial wavepacket and the target

$$\langle x_l|\psi^+_{+k}\rangle = \exp(\imath k x_l) + R\exp(-\imath k x_l) \ , \tag{48}$$

$$\langle x_l|\psi^+_{-k}\rangle = T\exp(-\imath k x_l) \ . \tag{49}$$

To obtain T and R, we consider two points to the right of the potential (say, x_{r1} and x_{r2}) and two points between the initial wavepacket and the potential (say, x_{l1} and x_{l2}), where the final states are calculated (using the various expressions presented in the previous section). This leads to

$$R = \frac{Aa_1 - Ba_2}{A^2 - B^2} \ , \tag{50}$$

$$T = \frac{a_1 - AR}{B} \ , \tag{51}$$

where

$$a_1 = \frac{\langle x_{l1}|G(E)|\chi(0)\rangle\exp(-\imath k x_{l1}) - \langle x_{l2}|G(E)|\chi(0)\rangle\exp(-\imath k x_{l2})}{\exp(-2\imath k x_{l1}) - \exp(-2\imath k x_{l2})},$$

$$a_2 = \frac{\langle x_{r1}|G(E)|\chi(0)\rangle\exp(\imath k x_{r1}) - \langle x_{r2}|G(E)|\chi(0)\rangle\exp(\imath k x_{r2})}{\exp(2\imath k x_{r1}) - \exp(2\imath k x_{r2})},$$

$$A = \frac{\langle x_{l1}|G(E)|\chi(0)\rangle\exp(\imath k x_{l1}) - \langle x_{l2}|G(E)|\chi(0)\rangle\exp(\imath k x_{l2})}{\exp(2\imath k x_{l1}) - \exp(2\imath k x_{l2})},$$

$$B = \frac{\langle x_{r1}|G(E)|\chi(0)\rangle\exp(-\imath k x_{r1}) - \langle x_{r2}|G(E)|\chi(0)\rangle\exp(-\imath k x_{r2})}{\exp(-2\imath k x_{r1}) - \exp(-2\imath k x_{r2})} \ .$$

4.2 Results for the large box (box 1)

To demonstrate the validity of the expressions in Eqs. (33)–(36), (38) and (39), the box size was first set at a large enough value that reflection of the wavefunction at the boundary was negligible (see box 1 in Table 2). Hence damping was not required and $S^{1/2}$ was set to the identity matrix. The Eckart barrier was centered in the middle of the box, with its width chosen so that it was effectively nonzero over a small region in the box (Table 2). The initial wavepacket was chosen to be a moving Gaussian wavepacket with width σ_0, average momentum k_{ave} and centered at the point x_0, i.e.,

$$\langle x|\chi(0)\rangle = \frac{1}{\sqrt{\sigma_0\sqrt{\pi}}}\exp\left(-\frac{x-x_0}{2\sigma_0^2}\right)\exp(\imath k_{ave}x) \ . \tag{52}$$

The specific values chosen may be found in Table 2.

The undamped Hamiltonian matrix was diagonalized using a routine in LAPACK [46]. The banded, Toeplitz nature of the DAF-represented Hamiltonian made this calculation relatively easy. The resulting eigenstates were used as discussed previously, and the relevant TIW states were calculated at four points, as outlined earlier, to obtain the transmission and reflection coefficients for a wide range of energies, both above and below the barrier height, including a few exactly equal to the eigenvalues of the box Hamiltonian. Typical results for these calculations compared with the respective analytical values are presented in Table 3.

For the Chebychev expansions, the values of T and R were calculated as a function of the number of terms, N, included in the polynomial expansion. A typical behavior is shown in Fig. 3. The unitarity (or the conservation of flux) condition, $|T|^2 + |R|^2 = 1$, was conserved only in the stable plateau region, and the values in this region were found to be in good agreement with the exact values in Table 3. On further increasing the number of Chebychev terms, the plateau disappeared and the behavior was oscillatory from then on owing to reflections from the boundaries reaching back to the final state analysis points. It was also interesting to note that the plateau for the transmission coefficient always lasted longer than the plateau for the

Table 2. Box sizes and related parameters

	Box 1	Box 2	Box 3	Box 4
Box Size	600 Å	185 Å	130.0 Å	130.0 Å
Box range	−300 to 300 Å	−92.5 to 92.5 Å	−65.2 to 65.2 Å	−65.2 to 65.2 Å
Δx[a]	0.4 Å	0.4 Å	0.4 Å	0.4 Å
N[b]	1501	463	326	326
Potential range	−24.8 to 24.8 Å	−24.8 to 24.8 Å	−24.8 to 24.8 Å	−24.8 to 24.8 Å
x_0[c]	−185.2 Å	−55.30 Å	−28.0 Å	0.0 Å
σ_0[c]	6.0 Å	1.0 Å	_[d]	_[d]
k_{ave}[c]	0.1732	0.1732	_[d]	_[d]
x_{l1}[e]	−25.6 Å	−25.6 Å	−25.6 Å	−25.6 Å
x_{l2}[e]	−26.4 Å	−26.4 Å	−26.4 Å	−26.4 Å
x_{r1}[e]	+25.6 Å	+25.6 Å	+25.6 Å	+25.6 Å
x_{r2}[e]	+26.4 Å	+26.4 Å	+26.4 Å	+26.4 Å
n_{damp}[f]	–	7	90	90

[a] Grid spacing
[b] Number of points on the grid
[c] Initial wavepacket parameters. See Eq. (52)
[d] Initial wavepacket nonzero only over one grid
[e] Final state analysis points
[f] Number of damping points on grid

Table 3. Results for box 1

Energy		Exact[a]	Chebychev expansions			$\delta_M(E-H\|\sigma)$	Finite-τ expansions		
			$G^+(E)$	$G^P(E)$	$\delta(E-H)$		$G^+(E)$	$G^P(E)$	$\delta(E-H)$
0.012[b]	$\|T\|^2$	0.166	0.166	0.166	0.166	0.167	0.167	–	–
	$\|R\|^2$	0.834	0.833	0.833	0.833	0.834	0.833	–	–
0.024[b]	$\|T\|^2$	0.559	0.559	0.559	0.559	0.559	0.559	0.559	0.559
	$\|R\|^2$	0.441	0.441	0.441	0.441	0.441	0.438	0.438	0.438
0.036[b]	$\|T\|^2$	0.838	0.838	0.838	0.838	0.838	0.840	0.838	0.838
	$\|R\|^2$	0.162	0.162	0.162	0.162	0.162	0.165	0.160	0.160
0.048[b]	$\|T\|^2$	0.944	0.944	0.944	0.944	0.944	0.946	0.946	0.946
	$\|R\|^2$	0.0558	0.0558	0.0558	0.0558	0.0558	0.0565	0.0565	0.0565
0.060[b]	$\|T\|^2$	0.980	0.978	0.980	0.980	0.980	0.980	0.980	0.980
	$\|R\|^2$	0.0204	0.0203	0.0200	0.0205	0.0205	0.0208	0.0208	0.0208
0.008902[c]	$\|T\|^2$	0.0959	0.0959	0.0959	0.0959	0.0960	0.0959	0.0959	0.0959
	$\|R\|^2$	0.904	0.904	0.904	0.904	0.905	0.904	0.904	0.904
0.019991[c]	$\|T\|^2$	0.414	0.423	0.423	0.423	0.423	0.420	0.421	0.419
	$\|R\|^2$	0.586	0.576	0.576	0.576	0.577	0.581	0.577	0.577
0.031193[c]	$\|T\|^2$	0.753	0.753	0.753	0.753	0.753	0.753	0.753	0.753
	$\|R\|^2$	0.247	0.247	0.247	0.247	0.0247	0.247	0.247	0.0247
0.044867[c]	$\|T\|^2$	0.927	0.929	0.929	0.929	0.927	0.929	0.929	0.929
	$\|R\|^2$	0.0735	0.0736	0.0735	0.0735	0.0735	0.0735	0.0735	0.0735
0.055357[c]	$\|T\|^2$	0.970	0.971	0.970	0.970	0.970	0.970	0.972	0.970
	$\|R\|^2$	0.0299	0.0300	0.0299	0.0299	0.0298	0.0300	0.0299	0.0300

[a] Values obtianed from analytically exact expressions
[b] Energies not eigenvalues of Hamiltonian
[c] Energies are eigenvalues of Hamiltonian

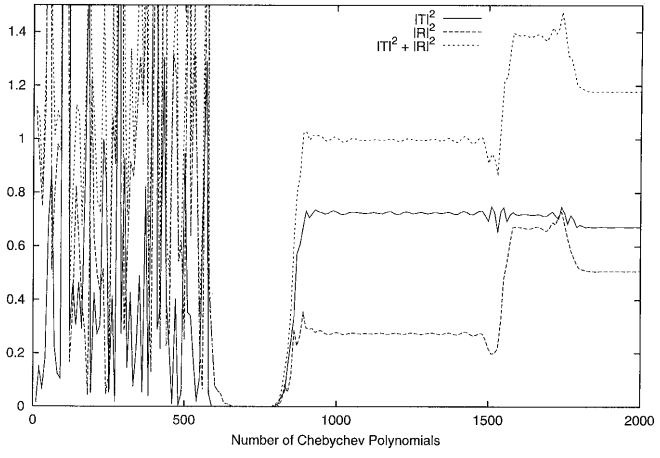

Fig. 3. Plot of $|T|^2$, $|R|^2$ and $|T|^2 + |R|^2$ as functions of the number of Chebychev polynomials for the case of the $G^P(E)$ in box 1, for energy equal to 0.030. Note the plateau around the range 1000–1500 Chebychev polynomials. Also note the plateau for $|T|^2$ (*solid line*) lasts slightly long than that for $|R|^2$ and $|T|^2 + |R|^2$. See text for details

reflection coefficient (Fig. 3). This was a direct reflection of the fact that boundary reflections arrive on the reflection side earlier than the transmission side, since the initial wavepacket was on the reflection side. (This also reflects the direct relationship between propagation time and order of Chebychev polynomials noted elsewhere [37].) The finite-τ expressions were studied as functions of τ. At low τ, the behavior was random but at larger values of τ, the transmission and reflection coefficients were found to exhibit regular oscillatory behavior (as seen in Fig. 4). The oscillations are damped with increasing values of τ and an average of the T and R values in this regular oscillatory region provides an estimate for the magnitude of the transmission and reflection coefficients which is in satisfactory agreement with the exact values, as seen in Table 3. Further, the unitarity condition was satisfied only in the regular oscillatory region and the more regular oscillations occur at smaller values of τ for the larger energies. This is due to the higher-energy components completing the collision process in a smaller propagation time (τ). The DAF representation for the spectral

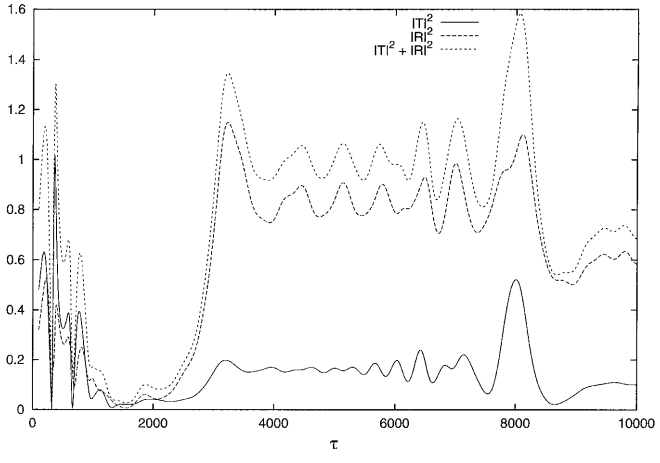

Fig. 4. Plot of $|T|^2$, $|R|^2$ and $|T|^2 + |R|^2$ as functions of τ for the finite-τ representation of $G^+(E)$ in box 1, energy equal to 0.012. Note the regular oscillatory region around the range 4000–7000 units on the τ axis

density operator, i.e., $\delta_M(E - H|\sigma)$, was studied as a function of the parameter σ, with the value of M being fixed at 60. A stable plateau was attained for all energy values. The position of the plateau shifted as a function of energy, with higher energies producing a plateau at higher σ values. This reflects the inverse relationship between the required propagation time and the value of σ, as noted in Sect. 3.1, using Fig. 1.

For all the calculations described previously, it was found that fewer than one-tenth of the eigenstates of the Hamiltonian were necessary at most scattering energies. The only exception to this was found to be the Chebychev-based approximations. Here the extremely low energy behavior was found to be oscillatory and unstable when fewer than one-tenth of the eigenstates were used, but stable when a larger number of eigenstates were used. The DAF approximation did not encounter this problem and gave rise to stable plateaus even at extremely low energies when fewer than one-tenth of the eigenstates were used. This difference in behavior is due to the fundamental difference between a DAF representation and the usual standard basis set expansion [47], of which the Chebychev polynomial approximation, considered earlier, is a very good example. While the leading error to a truncated Chebychev approximation of order N is a polynomial of order $N + 1$, which is oscillatory, this is not the case for the DAF expansion. The DAF approximation to a wide class of functions has been proved [47] to exhibit uniform convergence. This is unlike a standard basis set expansion approximation to a function which converges in the sense of the norm of the difference between the function and its approximation in the complete domain of definition of the function.

The fact that only a small number of eigenstates are necessary for these methods to yield reliable results is very interesting, since iterative techniques [7, 48–56] can be used to obtain a selected range of eigenstates. These methods have the advantage that the computational effort required scales linearly with system size (as opposed to the slow N^3 scaling of the standard eigenvalue solvers). In the present case, however, the lower dimensionality and the banded, Toeplitz nature of the DAF makes direct diagonalization feasible. For larger dimensional problems, however, iterative diagonalization should be the method of choice.

Having found all expressions to yield satisfactory results with the initial wavepacket on one side of the barrier, it was decided to place the initial wavepacket directly on top of the Eckart potential. (This, as will be seen in the next section, leads to an important consideration for box-size reduction, since if the initial wavepacket can be accommodated on top of the barrier and stable solutions obtained, the box size could be further reduced, hence reducing the size of the associated matrices involved.) It was found that the DAF expression gave an extremely stable plateau at all energies. The Chebychev and finite-τ expressions for $\delta(E - H)$, while yielding reasonably stable behavior, were not as stable as the results obtained using the DAF expression. Additionally, at lower energies the Chebychev and finite-τ expressions required a larger number of eigenstates to provide a reasonably stable plateau (as seen in the case with the initial wavepacket outside the barrier). Approximations to $G^+(E)$ and $G^{\mathrm{P}}(E)$ produced unstable results when the initial wavepacket was placed on top of the barrier.

We next carried out calculations for smaller box sizes in order to test the robustness of the approach. In the rest of this section, we consider the effect of reduction in box size on accuracy.

4.3 Results of calculations for smaller boxes (boxes 2, 3, 4): test of computational robustness

For smaller boxes, the plateaus typically were not stable and well-defined owing to multiple reflections caused by the boundaries. Hence, the Hamiltonian was damped and the polynomial expansions were smoothed, as discussed earlier. The diagonal-damping matrix, $S^{1/2}$, was defined to be equal to a damping function, f, close to the edges of the grid (over n_{damp} grid points). Various damping functions were considered. The DAF damping (Fig. 2) using the diagonal Fourier space form of DAF, i.e.,

$$f(i) = \exp\left\{-\frac{1}{2}\left[\sigma'\left(6 - \frac{3i}{n_{\mathrm{damp}} - 1}\right)\right]^2\right\} \times \sum_{k=0}^{M} \frac{1}{k!}\left\{\frac{1}{2}\left[\left(6 - \frac{3i}{n_{\mathrm{damp}} - 1}\right)\sigma'\right]^2\right\}^k , \qquad (53)$$

for the grid point $i = 1, \ldots, n_{\mathrm{damp}}$ (with $\sigma' = 2.5$ and $M = 60$) and the square root of a cosine function (i.e., $f(i) = \sqrt{\cos\left(\frac{\pi(i-1)}{2(n_{\mathrm{damp}}-1)} - \frac{\pi}{2}\right)}$) were found to work best and hence these are used for the calculations reported herein. The DAF was also used to smooth the polynomial expansions, as outlined earlier. The introduction of damping and smoothing produced stable plateaus for the DAF and Chebychev expressions and greatly improved the results obtained for the finite-τ expressions.

In the case of the Chebychev expansion, both the standard Chebychev recursion, Eq. (29), and the damped Faber–Chebychev recursion, Eq. (30), were tested. In box 2 both expressions lead to stable plateaus for all energies (including those that were exactly equal to the eigenvalues of the damped Hamiltonian) when the entire eigenspectrum of the Hamiltonian was used; however, as in box 1, when less than one-tenth of the eigenstates were used, the behavior was unstable for the lower energies. (Since the results for box 2 are similar to those obtained for box 1, we do not present them here.) For energies where a stable plateau was obtained, the width of the plateau was found to be smaller in box 2 than in box 1, but a smaller number of Chebychev terms were required to attain the plateau. This was simply due to a smaller box requiring a shorter time of propagation.

The DAF expansion, when used in box 2, yielded stable plateaus (for all energies) at σ values larger than those for which plateaus were obtained for box 1. This again reflects an inverse relationship between time of propagation and σ. Similarly, the τ expressions yielded regular oscillatory behavior at smaller values of τ.

These results encouraged us to reduce the box size further. Although several smaller boxes were studied, only the results for two such boxes are presented here (see boxes 3, 4 in Table 2). In box 3, the width of the initial wavepacket was reduced to one point and placed to the left of the barrier. The number of points in the damping region was increased to account for the greater reflection produced by the smaller box size and the smoothing constant σ' (in Eq. 32) was reduced to 0.0050 to provide greater filtering of the high-frequency noise produced by boundary reflections (Table 2). In addition, since the DAF representation of the kinetic energy operator in Eq. (44) ensured that the Hamiltonian was nonlocal to a maximum of 30 grid points, close to 30 grid points were maintained between the region of final state analysis and the damping region. This ensured that the Hamiltonian did not couple the final state analysis region with the damping region, and Eq. (31) was valid in all physical space. This resulted in stable plateaus for the DAF (Fig. 5) and Chebychev expansions (results for box 3 may be found in Table 4).

Next, the same initial wavepacket (nonzero at just one point, as in the case of box 3) was moved to the center of the Eckart barrier and the results were studied (box 4 in Table 2). Only the DAF and Chebychev approximations to the spectral density operator provided stable results (Figs. 6, 7). (Some of these results were even better than the ones obtained in box 3, i.e., with the initial wavepacket outside the barrier; Table 4). The $G^{\mathrm{P}}(E)$ expression was found to give qualitatively correct results only at energies above the barrier height, but the results in this case were not as accurate as those obtained using the expressions for the SDO.

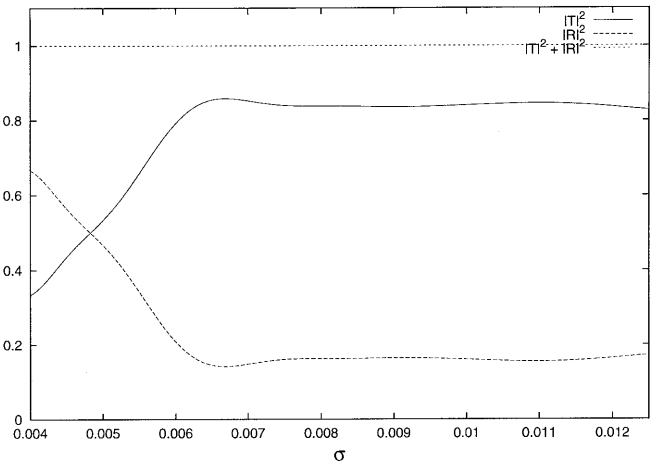

Fig. 5. Plot of $|T|^2$, $|R|^2$ and $|T|^2 + |R|^2$ as functions of σ for the case of the DAF representation of the spectral density operator (*SDO*) in box 3, for energy equal to 0.036. Note the stable plateau around the range 0.0075–0.01 units on the σ axis

5 Discussion

In this article we have considered various approximate solutions to the TIW, definite-energy Schrödinger equation. It is seen that a variety of functions can be defined and computed in order to obtain quantum scattering information. For example, Chebychev expansions of the infinite-τ causal, particular and homogeneous solutions can be constructed. Alternatively, one may also develop approximations to the homogeneous solution of the $\tau \to \infty$ TIW equation by approximating $\delta(E-H)$. An especially promising approximation is the DAF, $\delta_{\sigma,M}(E-H)$ [21]. Finite-τ propagation of an initial wavepacket can also be carried out; in this case the scattering process is studied as a function of the propagation time, τ. In all cases, the calculation strategies revolve around being able to calculate analytically the dependence on the scattering energy, E. This leads to efficient methods for computing scattering information at many energies.

All approximations studied here are made computationally robust and reliable by the introduction of damping and smoothing to facilitate smaller and more compact grids. The damped Hamiltonian approach may be used in conjunction with any of the approximations to the causal, particular or homogeneous solutions.

An important computational strategy that was used to test the various alternative schemes was the inclusion of only a fraction of the eigenstates of the discrete Hamiltonian matrix in an approximate resolution of the identity to evaluate the various TIW functions. It was found that to obtain scattering information at any energy, only a window of eigenstates around the scattering energy was required. This is particularly interesting since any of the novel iterative eigensolvers based on the Arnoldi/Lanczos idea [7, 48–56] can be used for this purpose. Of particular interest will be those that can be used to obtain accurate interior eigenstates [53]. It is also interesting to note the computational gains that may be afforded by the use of such iterative eigensolvers. For example, in box 1 a standard Chebychev propagation would require at least 1000 Chebychev vectors (i.e., 1000 matrix vector multiplies) to reach the base of the stable plateau. The iterative solvers would require roughly 200

Table 4. Boxes 3 and 4

Energy		Exact	Chebychev expansions				Distributed approximating functional expansions	
			$G^{+}(E)$[a]	$G^{P}(E)$[a]	$\delta(E-H)$[a]	$\delta(E-H)$[b]	$\delta_M(E-H\|\sigma)$[a]	$\delta_M(E-H\|\sigma)$[b]
0.012[c]	$\|T\|^2$	0.166[e]	0.157	0.131	0.169	0.162	0.159	0.168
	$\|R\|^2$	0.834	0.877	0.869	0.831	0.838	0.841	0.831
0.024[c]	$\|T\|^2$	0.559	0.539	0.574	0.534	0.540	0.550	0.558
	$\|R\|^2$	0.441	0.458	0.426	0.466	0.460	0.450	0.440
0.036[c]	$\|T\|^2$	0.838	0.839	0.840	0.839	0.839	0.838	0.838
	$\|R\|^2$	0.162	0.161	0.160	0.161	0.161	0.162	0.161
0.048[c]	$\|T\|^2$	0.944	0.947	0.947	0.947	0.947	0.940	0.944
	$\|R\|^2$	0.0558	0.0529	0.0531	0.0530	0.0532	0.0595	0.0556
0.060[c]	$\|T\|^2$	0.980	0.981	0.981	0.981	0.981	0.980	0.973
	$\|R\|^2$	0.0204	0.0186	0.0186	0.0186	0.0186	0.0198	0.0261
0.013033[d]	$\|T\|^2$	0.195	0.196	0.206	0.167	0.183	0.199	0.197
	$\|R\|^2$	0.805	0.830	0.794	0.833	0.817	0.801	0.803
0.020164[d]	$\|T\|^2$	0.429	0.399	0.307	0.404	0.398	0.425	0.428
	$\|R\|^2$	0.571	0.595	0.693	0.596	0.602	0.575	0.572
0.028754[d]	$\|T\|^2$	0.696	0.690	0.689	0.682	0.686	0.685	0.690
	$\|R\|^2$	0.304	0.312	0.311	0.318	0.314	0.315	0.304
0.038772[d]	$\|T\|^2$	0.874	0.876	0.875	0.877	0.875	0.877	0.875
	$\|R\|^2$	0.126	0.125	0.125	0.123	0.125	0.123	0.125
0.050187[d]	$\|T\|^2$	0.954	0.956	0.956	0.956	0.956	0.954	0.953
	$\|R\|^2$	0.0462	0.0436	0.0437	0.0436	0.0436	0.0457	0.0476

[a] Box 3
[b] Box 4
[c] Energies not eigenvalues of Hamiltonian
[d] Energies are eigenvalues of Hamiltonian

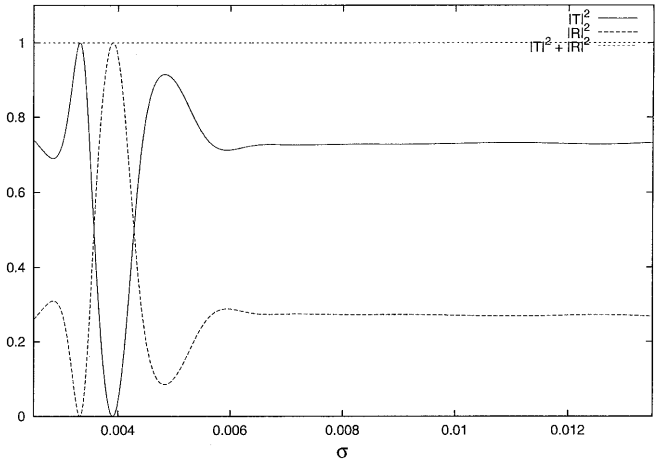

Fig. 6. Plot of $|T|^2$, $|R|^2$ and $|T|^2+|R|^2$ as functions of σ for the case of the DAF representation of the SDO in box 4, for energy equal to 0.030. Note the stable plateau around 0.01 units on the σ axis

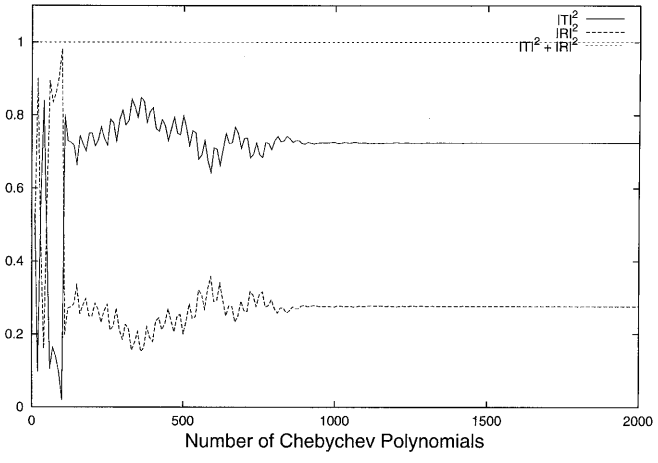

Fig. 7. Plot of $|T|^2$, $|R|^2$ and $|T|^2+|R|^2$ as functions of the number of Chebychev polynomials for the case of $\delta(E-H)$ in box 4, for energy equal to 0.030. Note the stable plateau beyond 1000 Chebychev polynomials

vectors (each generated from a matrix vector multiply) to obtain the window of eigenstates. Once this subset of eigenstates is obtained, it can be used to perform calculations at scattering energies close to the center of the window. This could lead to a computationally viable scheme for higher-dimensional systems and should be further explored.

Approximating the SDO using the Hermite–DAF leads to interesting results. Since the DAF is not a standard basis set expansion [21, 47], it has properties that differ, for example, from the Chebychev expansion. Of particular interest is the fact that the truncation error is not a higher-order polynomial for the DAF (as it is for the standard Chebychev expansion or for any other similar basis set expansion). The effect of this was seen clearly for box 1 when no smoothing was used. At low energies, the Chebychev polynomial expansion was found to be unstable when only a small fraction of the eigenstates were used, but became stable when a larger number of eigenstates were used. The DAF, on the other

hand, provided suitable results at all energies, always requiring only a small fraction of the eigenstates. The use of other DAFs, like the Gaussian–DAF–sinc operator [30], the Lagrange DAF [27–29] or the symmetry–adapted DAF (when the Hamiltonian has symmetry, which can be exploited to reduce its size) [31], may provide alternative, viable methods to evaluate scattering information.

It is also shown that all the approximations studied here are well behaved at all energies, including those equal to the exact eigenvalues of the finite-matrix Hamiltonian. This is very interesting, since there exists another approach, known as '**R**'-matrix theory, which is also based on diagonalization of the Hamiltonian; however, this method leads to a singular Green function at the eigenenergies of the Hamiltonian. This does not occur in the present approach since the correct limit of $\epsilon \rightarrow 0_{\pm}$ (to select causal or anticausal behavior) is implicit in all the expressions studied here.

Acknowledgements. S.S.I. would like to thank Troy Konshak for his helpful comments during this project. S.S.I. was supported in part under the R.A. Welch Foundation grant E-0608. D.J.K. was supported under the National Science Foundation grant CHE9700297. The Ames Laboratory is operated for the Department of Energy by Iowa State University under contract no. 2-7405-ENG82.

References

1. Zhang DH, Zhang JZH (1996) In: Wyatt RE, Zhang JZH (eds) Dynamics of molecules and chemical reactions. Dekker, New York, pp 231–276
2. Neuhauser D, Judson RS, Baer M, Kouri DJ (1994) In: Bowman JM (eds) Advances in molecular vibrations and collision dynamics, vol 2B. Jai, Greenwich, Conn., pp 27–44
3. Kosloff R (1994) Annu Rev Phys Chem 45: 145
4. Mowrey RC, Kouri DJ (1986) J Chem Phys 84: 6466
5. Goldberger ML, Watson KM (1964) Collision theory. Wiley, New York
6. Lippmann BA, Schwinger J (1950) Phys Rev 79: 469
7. Kouri DJ, Arnold M, Hoffman DK (1993) Chem Phys Lett 203: 166
8. (a) Huang Y, Zhu W, Kouri DJ, Hoffman DK (1993) Chem Phys Lett 206: 96; (b) Huang Y, Zhu W, Kouri DJ, Hoffman DK (1993) Chem Phys Lett 213: 209
9. Zhu W, Huang Y, Kouri DJ, Arnold M, Hoffman DK (1994) Phys Rev Lett 72: 1310
10. Hoffman DK, Huang Y, Zhu W, Kouri DJ (1994) J Chem Phys 101: 1242
11. Kouri DJ, Huang Y, Zhu W, Hoffman DK (1994) J Chem Phys 100: 3662
12. Hoffman DK, Kouri DJ, Top ZH (1979) J Chem Phys 70: 4640
13. Evans JW, Hoffman DK, Kouri DJ (1983) J Math Phys 24: 576
14. Fano U (1964) In: Cainiello ER (ed) Lectures on the many-body problem, vol 2. Academic, New York, p 217
15. Fano U (1963) Phys Rev 131: 259
16. Newton RG (1982) Scattering theory of waves and particles. Springer, Berlin Heidelberg New York
17. Bender CM, Orzag SA (1978) Advanced mathematical methods for scientists and engineers. McGraw-Hill, New York
18. Jang HW, Light JC (1995) J Chem Phys 102: 3262
19. (a) Mandelshtam VA, Taylor HS (1995) J Chem Phys 102: 7390 (b) Mandelshtam VA, Taylor HS (1995) J Chem Phys 103: 2903
20. (a) Chen R, Guo H (1996) J Chem Phys 105: 1311; (b) Chen R, Guo H (1996) J Chem Phys 105: 3596
21. Hoffman DK, Nayar N, Sharafeddin OA, Kouri DJ (1991) J Phys Chem 95: 8299
22. Hoffman DK, Kouri DJ (1992) J Phys Chem 96: 1179
23. Kouri DJ, Zhu W, Ma X, Pettitt BM, Hoffman DK (1992) J Phys Chem 96: 9622
24. Kouri DJ, Hoffman DK (1992) J Phys Chem 96: 9631
25. Hoffman DK, Arnold M, Kouri DJ (1992) J Phys Chem 96: 6539
26. Hoffman DK, Marchioro TL II, Arnold M, Huang Y, Zhu W, Kouri DJ (1996) J Math Chem 20: 117
27. Wei GW, Zhang DS, Kouri DJ, Hoffman DK (1997) Phys Rev Lett 79: 775
28. Zhang DS, Wei GW, Kouri DJ, Hoffman DK (1998) Chem Phys Lett 284: 56
29. Wei GW, Althorpe SC, Zhang DS, Kouri DJ, Hoffman DK (1998) Phys Rev A 57: 3309
30. Hoffman DK, Wei GW, Zhang DS, Kouri DJ (1998) Chem Phys Lett 287: 119
31. Iyengar SS, Parker GA, Kouri DJ, Hoffman DK (1999) J Chem Phys 110: 10283
32. Iyengar SS (1998) PhD thesis. University of Houston
33. (a) Hartke B, Kosloff R, Ruhman S (1986) Chem Phys Lett 158: 223; (b) Baer R, Kosloff R (1992) Chem Phys Lett 200: 183
34. Kosloff R (1998) J Phys Chem 92: 2087
35. Iyengar SS, Kouri DJ, Parker GA, Hoffman DK. Theor Chem Acc (in press)
36. Abramowitz M, Stegan IA (eds) (1964) Handbook of mathematical functions. U.S. Government Printing Office, Washington, DC
37. Huang Y, Iyengar SS, Kouri DJ, Hoffman DK (1996) J Chem Phys 105: 927
38. Huang Y, Kouri DJ, Hoffman DK (1994) Chem Phys Lett 225: 37
39. Huang Y, Kouri DJ, Hoffman DK (1994) J Chem Phys 101: 10493
40. Stechel EB, Walker RB, Light JC (1978) J Chem Phys 69: 3518
41. Daubechies I (1992) Ten lectures in wavelets. SIAM, Philadelphia
42. Powell JL, Crasemann B (1961) Quantum mechanics. Addison-Wesley Reading, Mass
43. Neuhauser D, Baer M, Judson RS, Kouri DJ (1990) J Chem Phys 93: 312
44. Seideman T, Miller WH (1992) J Chem Phys 96: 4412
45. Vibok A, Balint-Kurti GG (1992) J Chem Phys 96: 7615
46. Anderson E, Bai Z, Bischof CH, Demmel J, Dongarra JJ, Du Croz J, Greenbaum A, Hammerling S, Mckenney A, Ostrouchov S, Sorensen DC (1992) LAPACK user's guide. SIAM, Philadelphia
47. Chandler C, Gibson AG (1999) J Approx Theory 100: 233
48. Sorensen DC (1992) Soc Ind Appl Math J Matr Anal Appl 13: 357
49. Parlett BN, Saad Y (1987) Lin Alg Appl 88/89: 575–595
50. Nauts A, Wyatt RE (1983) Phys Rev Lett 51: 2238
51. Zhu W, Huang Y, Kouri DJ, Chandler C, Hoffman DK (1994) Chem Phys Lett 217: 73
52. Parker GA, Zhu W, Huang Y, Hoffman DK, Kouri DJ (1996) Comput Phys Commun 96: 27
53. Huang Y, Kouri DJ, Hoffman DK (1999) J Chem Phys 110: 8303
54. Neuhauser D (1994) J Chem Phys 100: 5076
55. Chen R, Guo H (1997) Chem Phys Lett 277: 191
56. Mandelshtam VA, Taylor HS, Miller WH (1996) J Chem Phys 105: 496